J. Fluid Mech. (1995), *vol.* 294, *pp.* 209–230

Thermocapillary migration of a two-dimensional liquid droplet on a solid surface

By MARC K. SMITH

The George W. Woodruff School of Mechanical Engineering, Georgia Institute of Technology, Atlanta, GA 30332-0405, USA

(Received 15 October 1993 and in revised form 28 December 1994)

A two-dimensional liquid droplet placed on a non-uniformly heated solid surface will move towards the region of colder temperatures if the temperature gradient in the solid surface is large enough. Such behaviour is analysed for a thin viscous droplet using lubrication theory to develop an evolution equation for the shape of the droplet. For the small mobility capillary numbers examined in this work, the contact-line motion is controlled by a dynamic relationship posed between the contact-line speed and the apparent contact angle. Results are obtained numerically and also approximately using a perturbation technique for small heating. The initial spreading or shrinking of the droplet when placed on the heated solid is biased toward the direction of decreasing temperature on the solid. Possible steady-state responses are either a motionless droplet or one moving at a constant velocity down the temperature gradient without change in shape. These behaviours are the result of a thermocapillary recirculation cell inside the droplet that distorts the free surface and alters the apparent contact angles. This change in the apparent contact angles then modifies the contact-line speed.

1. Introduction

Thin liquid films and droplets are important elements in some heat transfer equipment designs such as heat exchangers, evaporators, condensers, and heat pipes. It is important to know how such thin liquid masses behave in these devices, especially with regard to the thermal fields that are present. Thus, the spreading of droplets and films and the influence of imposed temperature fields is a research area of fundamental importance.

When a liquid droplet is placed on a smooth isothermal solid surface it will spread or contract to an equilibrium shape in which the capillary and hydrostatic pressure fields are balanced inside the droplet. The behaviour of the liquid during the spreading process is controlled by the motion of the contact lines where the liquid, the solid, and the bounding gas meet. The importance of this contact-line region and the difficulties in modelling it have been well reviewed by Dussan V. (1979) and de Gennes (1985). This region and its effect on the overall motion of the droplet can be modelled in several different ways, as discussed by Ehrhard & Davis (1991). One way is to allow the fluid to slip at the contact line. This condition is *ad hoc*, but it relieves a stress singularity that appears in the flow field if the no-slip boundary condition is used. In addition to slip, a condition for the *actual* contact angle (measured on a micron-sized slip-length scale) versus the contact-line speed must be specified. Using these conditions, the flow field very near the contact line is found and then matched to the flow in the bulk of the droplet. One major debate about this slip model is concerned with the form of the contact-angle condition. One could use a static condition in which

the contact angle is fixed at its equilibrium value for all contact-line speeds, or a dynamic condition in which the actual contact angle varies with speed. Hocking (1992) compared the static and the dynamic contact-angle conditions and concluded that given a specific form of the dynamic condition, both models can predict the observed behaviour of a spreading droplet. He then argued that given no specific experimental evidence for this choice of the dynamic condition, there is no reason to use it and so the simpler static condition should be used instead.

Another modelling technique for the contact-line region is based on the idea that a thin precursor film extends ahead of the apparent contact line of the droplet. Molecular effects are important in this thin film, and will essentially control the motion of the main body of the droplet over the solid surface. In this approach, there is no real contact line, only an apparent contact line and an apparent contact angle because the precursor film is too thin to see.

The last modelling scheme is to represent the entire contact-line region with an effective dynamic contact-line condition imposed on the bulk droplet. This approach is useful when only the bulk fluid motion is of interest and it can actually encompass the previous two models. The basis of the model is to examine the fluid motion very near to the real or apparent contact line and to characterize it either theoretically or experimentally. Then an effective boundary condition for the velocity of the contact line as a function of the *apparent* contact angle (measured on a millimetre-sized capillary-length scale) is constructed. This condition is used to drive the motion of the fluid in the bulk of the droplet. In this model, the entire effect of the small-scale physics near the contact line, whether it is slip, a precursor film, or anything else, is communicated to the bulk of fluid via the dynamic contact-line boundary condition. The small-scale physics does not need to be considered anywhere else. Hocking (1992) derived such a dynamic condition from the slip model and de Gennes (1985) derived it from the precursor-film model. The series of papers by Ngan & Dussan V. (1989), Dussan V., Ramé & Garoff (1991), and Marsh, Garoff & Dussan V. (1993) investigated this dynamic contact-line boundary condition experimentally. Their results show that a geometry-independent relation involving the apparent contact angle is impossible, but that a dynamic contact-line condition involving an intermediate contact angle measured on a length scale somewhere between those used to measure the apparent and the actual contact angle is possible. Note that a model using a dynamic contact-line boundary condition based on the apparent contact angle and a slip model using a dynamic contact-angle relation for the actual contact angle can produce identical results to leading order. This fact has produced some confusion in interpreting the results of these models.

We shall use this third approach in the present paper. We assume for a specific liquid, solid, and gas combination in a specific geometry that the proper dynamic contact-line boundary condition can be found, either experimentally or analytically. We use an apparent contact angle in this relation and remember that it applies only to the specific geometry under consideration. Once this dynamic contact-line condition is in hand, the bulk motion of a thin viscous droplet is determined by examining only the motion in the bulk of the droplet. The small-scale details of the flow very near the contact line will not be considered. The resulting leading-order approximation is much simpler to deal with and should adequately describe the bulk motion of the droplet.

The spreading droplet problem has been well-studied by a number of different authors. Hocking (1983), Hocking & Rivers (1982), and Haley & Miksis (1991) have examined an isothermal droplet spreading under the influence of gravity and capillarity. This work involves the use of a slip boundary condition at the contact line,

local solutions near the contact line, and global matching to determine the motion of the bulk droplet. Ehrhard & Davis (1991) extended this model by considering a spreading droplet with uniform heating or cooling of the solid surface. In their work, they used a slip model with the dynamic contact-angle relation for the motion of the contact line discussed by Dussan V. (1979). Their results showed that when the solid is heated, a thermocapillary flow forms that is directed from the contact lines towards the top of the droplet. This flow reduces the contact angles and inhibits spreading. Cooling the solid has exactly the opposite effect.

Greenspan (1978) also considered the spreading of a thin droplet on a horizontal surface, but used a simpler dynamic model than the one used by Ehrhard & Davis (1991). He also considered a coated surface in which the equilibrium contact angle decreased with distance. With this model, he showed that a droplet could be made to migrate down the plate in the direction of decreasing equilibrium contact angle. Chaudhury & Whitesides (1992) showed experimentally that this kind of behaviour is possible by making a droplet of water move uphill on a coated inclined plate.

The present paper generalizes the work of Ehrhard & Davis (1991) to include a migration effect similar to that seen by Greenspan (1978). A thin two-dimensional liquid droplet on a *non-uniformly* heated horizontal plate is considered. In particular, the temperature of the plate decreases linearly in one direction. This heating produces a themocapillary flow inside the droplet that modifies the contact angles. We use the same dynamic contact-angle relation used by Ehrhard & Davis (1991), but since we are only concerned with the leading-order motion of the bulk droplet we pose the relation with respect to the apparent rather than the actual contact angle. We shall show that the spreading process is altered considerably by the heating, and that migration of the entire droplet down the temperature gradient is possible.

In §2, the formulation of the model is presented and scaled in terms of the lubrication variables for a thin droplet. These governing equations are then solved to leading order for a thin droplet to produce an evolution equation for the shape of the free surface. This in turn is simplified by taking the limit of either a small spreading rate or a large surface tension. The result is a nonlinear equation for the shape of the free surface. We describe the solution of this equation both asymptotically and numerically in §3. When this solution is coupled to the dynamic contact-line boundary condition, the result describes the overall motion of the contact lines and therefore the bulk droplet motion. These results are presented in §4. Our conclusions are summarized in §5.

2. Formulation

2.1. *Basic governing equations*

Consider a two-dimensional liquid droplet on a horizontal non-uniformly heated solid surface, as shown in figure 1. A Cartesian coordinate system is used with the x-axis embedded in the solid surface and the z-axis normal to the solid surface. The droplet is composed of an incompressible Newtonian liquid with density ρ, dynamic viscosity μ, specific heat c_p, and thermal conductivity k. It is bounded above by a passive gas at the temperature T_∞ that can convectively heat or cool the droplet. The velocity $\boldsymbol{v} = (u, w)$, pressure p, and temperature T in the droplet are governed by the Navier–Stokes, continuity, and energy equations,

$$\rho\{\boldsymbol{v}_t + (\boldsymbol{v}\cdot\boldsymbol{\nabla})\boldsymbol{v}\} = -\boldsymbol{\nabla}p - \rho g\boldsymbol{k} + \mu\boldsymbol{\nabla}^2\boldsymbol{v}, \tag{1a}$$

$$\boldsymbol{\nabla}\cdot\boldsymbol{v} = 0, \quad \rho c_p\{T_t + \boldsymbol{v}\cdot\boldsymbol{\nabla}T\} = k\boldsymbol{\nabla}^2 T, \tag{1b, c}$$

where $\boldsymbol{k} = (0, 1)$ is a unit vector in the z-direction.

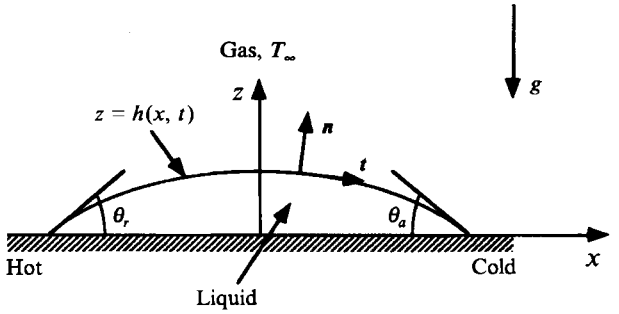

FIGURE 1. The geometry of a two-dimensional liquid droplet.

The free surface of the liquid is located at $z = h(x, t)$. The boundary conditions imposed on this surface are the kinematic condition, the normal- and tangential-stress balances, and an energy balance as follows:

$$w = h_t + uh_x, \quad \boldsymbol{t}\cdot\boldsymbol{S}\boldsymbol{n} = \boldsymbol{t}\cdot\nabla\sigma, \quad \boldsymbol{n}\cdot\boldsymbol{S}\boldsymbol{n} = -\sigma\kappa, \quad -k\nabla T\cdot\boldsymbol{n} = h_g(T - T_\infty). \quad (2a\text{–}d)$$

Here, $\boldsymbol{S}$ is the stress tensor for the liquid, σ is the surface tension of the free surface, h_g is the convection heat transfer coefficient for the free surface, and the subscripts x and t refer to partial differentiation. The unit normal and tangent vectors, $\boldsymbol{n}$ and $\boldsymbol{t}$, and the curvature of the free surface κ in these boundary conditions are defined as

$$\boldsymbol{n} = (-h_x, 1)/(1 + h_x^2)^{1/2}, \quad \boldsymbol{t} = (1, h_x)/(1 + h_x^2)^{1/2}, \quad \kappa = -h_{xx}/(1 + h_x^2)^{3/2}. \quad (3a\text{–}c)$$

The effect of thermocapillarity is modelled by assuming that the surface tension depends linearly on the temperature of the liquid

$$\sigma = \sigma_0 - \gamma(T - T_0), \quad (4)$$

where $\gamma > 0$ is the negative of the rate of change of surface tension with temperature, T_0 is the reference temperature, and σ_0 is the surface tension at the reference temperature.

The boundary conditions imposed on the solid surface at $z = 0$ are the slip condition, the no-penetration condition, and a fixed-temperature-gradient condition,

$$u = \beta' \partial u/\partial z, \quad w = 0, \quad T = T_0 - bx, \quad (5a\text{–}c)$$

where β' is the slip coefficient and $b = -\mathrm{d}T/\mathrm{d}x$ is the imposed temperature gradient. Although slip is not needed in our model for the droplet motion *away* from the contact lines, we include it at this stage for comparison to previous and related work on spreading droplets with the slip model.

The contact line on the right is located at the point $x = c_a(t)$ and the one on the left is at $x = c_r(t)$. The conditions of contact for the free surface at these points are

$$h(c_a, t) = 0, \quad h(c_r, t) = 0. \quad (6a, b)$$

The apparent contact angles θ_a and θ_r at the corresponding contact lines are found from the relations

$$h_x(c_a, t) = -\tan\theta_a(t), \quad h_x(c_r, t) = \tan\theta_r(t). \quad (6c, d)$$

At each contact line, the fluid velocity is equated to the velocity of the contact line

U_{cl}. The relationship between the contact-line speed and the *actual* contact angle discussed by Dussan V. (1979) and used by Ehrhard & Davis (1991) is

$$U_{cl} = \begin{cases} K(\theta - \theta_A)^m, & \theta > \theta_A, \\ -K(\theta_R - \theta)^m, & \theta < \theta_R, \end{cases} \tag{6e}$$

where K and m are constants, and θ_A and θ_R are the advancing and receding static contact angles. We pose this relationship at each contact line using the *apparent* contact angle.

The last condition imposed is that the volume of the droplet V_0 remains constant,

$$V_0 = \int_{c_r(t)}^{c_a(t)} h(x,t)\,\mathrm{d}x. \tag{7}$$

2.2. *Scaling*

The differential equations and boundary conditions (1)–(7) together with the appropriate initial conditions on the shape and position of the droplet completely define the motion of the droplet. To facilitate a solution of these equations in the limit of a thin droplet, scaling similar to those of Ehrhard & Davis (1991) are used as follows:

$$\left.\begin{aligned} x^* = \frac{x}{L}, \quad z^* = \frac{z}{L\theta_s}, \quad t^* = \frac{t}{L/K\theta_s^m}, \quad u^* = \frac{u}{K\theta_s^m}, \\ w^* = \frac{w}{K\theta_s^{m+1}}, \quad p^* = \frac{p}{\mu K\theta_s^{m-2}/L}, \quad T^* = \frac{T-T_\infty}{T_0-T_\infty}, \quad \theta^* = \frac{\theta}{\theta_s}. \end{aligned}\right\} \tag{8}$$

Here, $\theta_s = \theta_A$ is chosen as a measure for the contact angles in this problem, $L = (V_0/\theta_s)^{1/2}$ is a length scale based on the constant volume of the droplet, the velocity scale is based on the contact-line speed, and a convective time scale and a viscous pressure scale are used.

The dimensionless groups that arise from this scaling, appropriate to the evolution equation that follows, are the Bond number $G = \rho g L^2/\sigma_0$, the Biot number $B = h_g L\theta_s/k$, the mobility capillary number $C = \mu K/(\sigma_0\theta_s^{3-m})$, the thermocapillary number

$$\Delta C = \mu K/[\gamma(T_0 - T_\infty)\,\theta_s^{1-m}],$$

the slip number $\beta = \beta'/(\theta_s L)$, and the dimensionless imposed temperature gradient $N = bL/(T_0 - T_\infty)$. For clarity, we shall use $\bar{\theta}_A = 1$ as the scaled advancing contact angle and $\bar{\theta}_R$ as the scaled receding contact angle.

2.3. *Evolution equation*

The equations and boundary conditions (1)–(7) are made dimensionless with the scales given in (8). From here on, all variables are considered dimensionless and the asterisk superscript is dropped for simplicity. The thin-drop limit $\theta_s \to 0$ is used to obtain the appropriate lubrication equations. These are the same as the equations presented in Ehrhard & Davis (1991), except for the prescribed temperature condition on the solid surface $z = 0$,

$$T = 1 - Nx. \tag{9}$$

These lubrication equations describe a horizontal inertialess flow in the droplet driven by the horizontal gradient of the hydrostatic pressure and the thermocapillary stress on

the free surface, a vertical velocity determined through continuity, a hydrostatic pressure field determined by the height of the droplet and the capillary pressure at the free surface, and a conduction-dominated vertical heat transfer through the droplet.

The evolution equation for the shape of the droplet is derived from these lubrication equations. It is essentially a vertically averaged continuity equation of the form $h_t + q_x = 0$, where q is the net longitudinal flow in the droplet. For the present problem, this evolution equation is

$$Ch_t + \left\{(h_{xx} - Gh)_x(\tfrac{1}{3}h^3 + \beta h^2) + \frac{C}{\Delta C}\left(\frac{N}{1+Bh} + \frac{Bh_x(1-Nx)}{(1+Bh)^2}\right)(\tfrac{1}{2}h^2 + \beta h)\right\}_x = 0. \quad (10)$$

The corresponding velocity, pressure, and temperature in the droplet are

$$u = p_x[\tfrac{1}{2}z^2 - h(z+\beta)] + S\Delta C^{-1}(z+\beta), \quad (11a)$$

$$w = -p_{xx}[\tfrac{1}{6}z^3 - h(\tfrac{1}{2}z^2 + \beta z)] + p_x h_x(\tfrac{1}{2}z^2 + \beta z) - S_x \Delta C^{-1}(\tfrac{1}{2}z^2 + \beta z), \quad (11b)$$

$$p = -C^{-1}[h_{xx} + G(z-h)], \quad (11c)$$

$$T = (1-Nx)[1 + B(h-z)]/(1+Bh), \quad (11d)$$

with the quantity S defined as

$$S = \frac{N}{1+Bh} + \frac{Bh_x(1-Nx)}{(1+Bh)^2}. \quad (11e)$$

The shape of the droplet and its motion along the solid surface are described by the solution of the evolution equation (10), together with the corresponding dimensionless forms of the contact-line conditions (6), the constant-volume condition (7), and the appropriate initial conditions. Once this is known, the velocity, pressure and temperature fields are computed from (11).

2.4. *The limit of small mobility capillary number*

The spreading rates of interest in many problems are on the order of microns per second, resulting in mobility capillary numbers that are very small. This justifies an examination of the evolution equation (10) in the limit of $C \to 0$. The formal limit removes the time-derivative term in the evolution equation making it a nonlinear equation determining a steady droplet shape for a given droplet width. The droplet evolves as the contact lines move according to the dynamic condition (6*e*). This motion alters the width of the droplet and with it the shape of the free surface. This kind of quasi-steady evolution was discussed by Rosenblat & Davis (1985). Ehrhard & Davis (1991) used this limit to examine the quasi-steady evolution of a uniformly heated droplet. The small-C limit also neglects a small initial layer in time during which the free surface evolves from an arbitrary initial shape to the shape given by the leading-order approximation. This evolution is of no interest in this work.

A further consequence of the small-mobility-capillary-number limit involves the modelling assumptions in the contact-line region. For the slip model with a dynamic variation of the *actual* contact angle, the leading-order approximation of the droplet shape is one of no contact-line motion. With the contact lines fixed, the singularity associated with a moving contact line disappears and so slip is not needed. Thus, the slip number β can be set to zero and the actual contact angle is identical to the apparent contact angle. The contact-line motion is then driven by a dynamic boundary

condition that is identical to that used in the dynamic contact-line boundary condition model. In other words, both contact-line models are identical to leading order in this small-mobility-capillary-number limit and we shall not differentiate between the actual and the apparent contact angles any further. However, if the solution for the free-surface shape was pursued as a perturbation expansion in C, slip would be needed beyond the leading-order approximation in the slip model, and the second model would need a dynamic contact-line boundary condition valid to this next order.

Two further simplifications are used. The first is that the Biot number is very small, since the droplets under consideration are very small. The second is that $Nx \ll 1$. This is equivalent to saying that the temperature difference in the droplet from end to end is smaller than the temperature difference between the average temperature in the droplet and the temperature of the surrounding gas. Note that if the same temperature gradient is imposed on both the solid and the gas above the droplet, but slightly shifted so that there is always a constant temperature difference between the two, then the single assumption that the Biot number is small would result in the same simplified evolution equation given below. No restrictions on the imposed temperature gradient would be needed.

The evolution equation (10) with $C \to 0$ is now integrated once to yield $q = C_1$. At this order the droplet shape is steady and so the constant of integration must be zero by conservation of mass. The resulting equation with the above parameter simplifications is

$$(h_{xx} - Gh)_x + \tfrac{3}{2}(\hat{N} + \hat{M}h_x)h^{-1} = 0, \tag{12a}$$

with the parameters

$$\hat{N} = CN/\Delta C \quad \text{and} \quad \hat{M} = CB/\Delta C. \tag{12b}$$

Equation (12a) for the droplet shape is autonomous in x. To simplify the corresponding boundary conditions, the origin is redefined to lie on the centreline of the droplet $\bar{c}(t) = \frac{1}{2}(c_a + c_r)$, and $a(t) = \frac{1}{2}(c_a - c_r)$ is defined to be the half-width of the droplet. The shape equation (12a) is then solved subject to the contact conditions

$$h(-a) = 0, \quad h(a) = 0, \tag{12c, d}$$

and the constant-volume condition

$$1 = \int_{-a}^{a} h(x)\,\mathrm{d}x. \tag{12e}$$

Once the shape of the droplet is known, the two contact angles are found from the relations

$$\theta_a(t) = -h_x(a), \quad \theta_r(t) = h_x(-a). \tag{13a, b}$$

The right contact line is then advanced in time according to the relation

$$\frac{\mathrm{d}c_a}{\mathrm{d}t} = \begin{cases} (\theta_a - \bar{\theta}_A)^m, & \theta_a > \bar{\theta}_A \\ -(\bar{\theta}_R - \theta_a)^m, & \theta_a < \bar{\theta}_R, \end{cases} \tag{13c}$$

and the left contact line according to

$$\frac{\mathrm{d}c_r}{\mathrm{d}t} = \begin{cases} -(\theta_r - \bar{\theta}_A)^m, & \theta_r > \bar{\theta}_A \\ (\bar{\theta}_R - \theta_r)^m, & \theta_r < \bar{\theta}_R. \end{cases} \tag{13d}$$

The time variation of the half-width and the centreline position are found by integrating (13c) and (13d) and using the definitions of $a(t)$ and $\bar{c}(t)$.

3. Solution methods

3.1. *Asymptotic solution*

The shape equation and boundary conditions in (12) with $G = 0$ are solved using a regular perturbation expansion for small $\hat{M}$ and $\hat{N}$. The resulting approximation for the shape of the droplet is

$$h = \frac{3(a^2-x^2)}{4a^3} + \hat{M}\{x^2-a^2+\tfrac{3}{2}(a^2+x^2)\ln(2a)-\tfrac{3}{4}(a-x)^2\ln(a-x)-\tfrac{3}{4}(a+x)^2\ln(a+x)\} + \hat{N}\{2a^3x\ln(2a)+\tfrac{1}{2}a^2(a-x)^2\ln(a-x)-\tfrac{1}{2}a^2(a+x)^2\ln(a+x)\} + \hat{M}\hat{N}\{\tfrac{2}{3}a^6x\ln(2a)+\tfrac{1}{6}a^5(a-x)^2\ln(a-x)-\tfrac{1}{6}a^5(a+x)^2\ln(a+x)\}+\ldots. \quad (14)$$

The front and rear contact angles are

$$\theta_a = \frac{3}{2a^2}-\tfrac{1}{2}a\hat{M}+a^3\hat{N}+\tfrac{1}{3}a^6\hat{M}\hat{N}+\ldots, \quad \theta_r = \frac{3}{2a^2}-\tfrac{1}{2}a\hat{M}-a^3\hat{N}-\tfrac{1}{3}a^6\hat{M}\hat{N}+\ldots. \quad (15a, b)$$

We recover the result of Ehrhard & Davis (1991) when $\hat{N} = 0$.

3.2. *Numerical solution*

A numerical solution for the free-surface shape was obtained by solving the nonlinear differential equation (12*a*) iteratively using a Newton–Kantorovich method as described by Boyd (1989). Briefly, (12*a*) was differentiated with respect to h, h_x, and h_{xxx}, and then expanded in a Taylor series with respect to these three functions. The series was truncated after the linear terms and set to zero to form a third-order linear differential equation for Δ, the difference between the true solution and the current approximate solution. The coefficients of this equation depend on the current approximate solution. The difference function Δ was expanded in a set of basis functions based on Chebyshev polynomials. These basis functions were formulated to satisfy the contact conditions (12*c*, *d*) and the constant-volume condition (12*e*). The linearized equation is then solved using standard pseudospectral methods. The result is added to h to form the next approximate solution. The iteration is continued until convergence, which is when the sum of the absolute value of Δ at all collocation points is less than 10^{-10}. Fifty or one hundred collocation points were used in the results reported in this work.

The numerical solution of the droplet shape with 50 basis functions was compared to the exact result of Hocking (1983) for an isothermal droplet. With $G = 2$ and $a = 1$ or 2, the difference was less than 10^{-15} at each collocation point. This was an easy test because there is no singularity at the contact line for this case.

Next, the numerical results with 50 basis functions were compared to the perturbation approximation obtained above. For small $\hat{M}$, $\hat{N} = 0$, and $a = 1$, the difference in the droplet shape behaved like $O(\hat{M}^2)$ and was less than 10^{-4} for $\hat{M} = 0.1$. The difference in the contact angles behaved like just less than $O(\hat{M}^2)$ and was about 10^{-3} for $\hat{M} = 0.1$. For small $\hat{N}$, $\hat{M} = 0$, and $a = 1$, the difference in the droplet shape behaved like $O(\hat{N}^2)$ and was less than 1.5×10^{-4} for $\hat{N} = 0.1$. The difference in the contact angles behaved like just less than $O(\hat{N}^2)$ and was about 2×10^{-3} for $\hat{N} = 0.1$. For larger values of the droplet width the actual errors for both cases are worse than before, but they are still asymptotically correct for small $\hat{M}$ and $\hat{N}$.

Some results based on the numerical solution and the asymptotic approximation are compared graphically in the figures discussed in the next section. These figures show the extent of validity of the asymptotics.

4. Results

The purpose of this paper is to describe the motion of the contact lines of the droplet in response to the non-uniform heating of the solid surface. Given the way the present model has been posed, the contact-line motion is entirely determined by the apparent contact angles. These in turn are influenced by the flow field in the droplet. Ehrhard & Davis (1991) studied the case in which $\hat{N} = 0$ and $\hat{M} \neq 0$, a uniform heating or cooling of the solid surface. When the solid is heated, the temperature decreases along the free surface of the droplet from each contact line to the top of the droplet. This produces two thermocapillary recirculation cells in the droplet, with the flow along the free surface directed towards the top of the droplet, and the flow along the solid surface directed towards the contact lines. This flow tends to reduce the two contact angles, which then consequently reduces the contact-line speed and inhibits spreading. The shape of the droplet for this case remains symmetric.

Now, consider an imposed temperature gradient on the solid surface $\hat{N} > 0$ and no overall heat transfer to the overlying gas $\hat{M} = 0$. Here, the temperature decreases along the free surface of the droplet from the left contact line all the way to the right contact line. This produces a thermocapillary surface flow in the droplet directed from the left to the right contact line. As the surface flow moves toward the right contact line, the fluid is deflected by the solid to form a return flow along the solid surface that is directed back toward the left contact line. This results in single themocapillary recirculation cell rotating in the clockwise sense. Such a flow ensures that there is conservation of mass in the quasi-steady motion of the droplet. The pressure field driving this return flow causes the right end of the droplet to bulge outward, which increases the right contact angle, while the left end of the droplet bulges inward so that the left contact angle decreases. It is through these changes that the contact-line speed is modified.

The results discussed in this section all depend on the degree to which the thermocapillary flows described above modify the contact angles. For simplicity in the discussion, a number of system parameters are fixed. There is no gravity $G = 0$ unless otherwise stated, $\bar{\theta}_A = 1$ from the scaling of this problem, and $\bar{\theta}_R = 0.8$ is the receding contact angle except where noted. The spreading exponent $m = 3$ is chosen because it agrees with the spreading experiments of Tanner (1979), Chen (1988), and Ehrhard (1993), it agrees with the experiments of Marsh *et al.* (1993), it is suggested by the analysis of Hocking (1992) and de Gennes (1985), and because it was also used in the analysis of Ehrhard & Davis (1991).

4.1. *Initial response*

Consider an *isothermal* system composed of the droplet, the solid surface, and the surrounding gas. In this system, the droplet will spread to an equilibrium configuration in which both contact angles equal the advancing contact angle. From the contact-angle relations (15), the droplet half-width in this situation is

$$a = (3/(2\bar{\theta}_A))^{1/2} = (3/2)^{1/2}. \tag{16}$$

With the droplet in this equilibrium configuration, the solid is heated at time zero by imposing a constant temperature gradient on its surface. Because of the droplet's small mobility capillary number, the velocity and temperature fields within the droplet and the droplet shape reach their steady-state values based on the initial droplet width before either of the contact lines move. In terms of the motion of the contact lines, this droplet shape is called the initial shape. The motion of the contact lines is driven by the initial shape according to the relations (13*c*, *d*). If the contact angle is larger than the

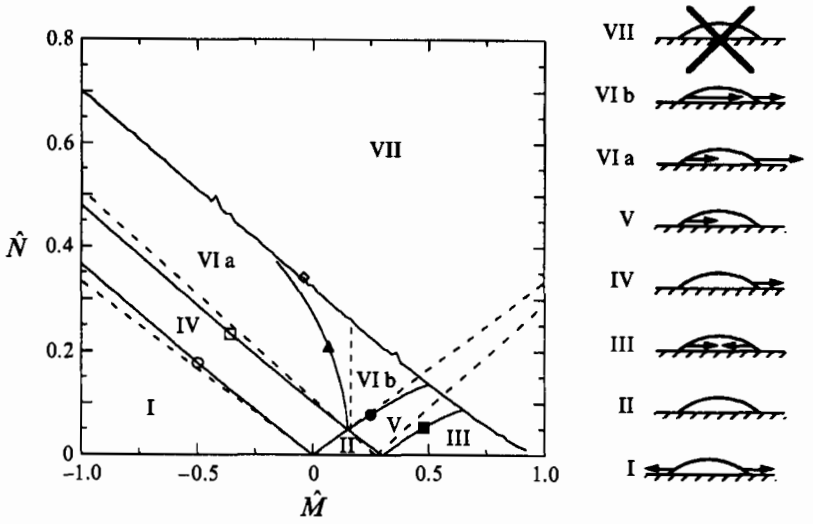

FIGURE 2. Parameter plot for the initial behaviour of a droplet with $G = 0$, $\bar{\theta}_A = 1$, and $\bar{\theta}_R = 0.8$. Solid lines are the numerical results and dashed lines are the asymptotic approximations. The marked regions are: I, two-sided spreading; II, no motion; III, two-sided shrinking; IV, one-sided spreading; V, one-sided shrinking; VIa, droplet migration with spreading; VIb, droplet migration with shrinking; and VII, invalid model behaviour. The curves are marked as follows: ○, $\theta_r = \bar{\theta}_A$; □, $\theta_r = \bar{\theta}_R$; ◇, $\theta_r = 0$; ●, $\theta_a = \bar{\theta}_A$; ■, $\theta_a = \bar{\theta}_R$; ▲, $\theta_a - \bar{\theta}_A = \bar{\theta}_R - \theta_r$. The small droplet schematics to the right of the figure indicate the direction and relative magnitude of the contact-line motion in each of the marked regions.

advancing angle, the contact line is said to advance, if it is between the advancing and receding contact angle, the contact line is motionless, or pinned, and if the contact angle is less than the receding angle, the contact line recedes.

The possible initial responses for the droplet described above are shown in figure 2. In this figure, the solid lines represent the results of numerical calculations and the dashed lines are found from the perturbation approximation. The lines are the result of finding the value of $\hat{N}$ for a fixed droplet width and a given $\hat{M}$ for which the right or left contact angle equals the advancing or receding contact angle or zero, or when they satisfy an equal-velocity condition as indicated in the figure caption. The equations for the lines obtained from the perturbation approximation are shown in the Appendix. Note that the asymptotic results are quite good near the origin of the plot as expected, but they deviate from the numerical results for large values of $\hat{M}$ and $\hat{N}$. The solid lines divide the figure into seven regions. The small droplet schematics to the right of the figure indicate the direction and relative magnitude of the contact-line motion in each of these regions.

First, if both contact angles are larger than the advancing contact angle of the droplet, then both contact lines will advance away from the centre of the droplet. This is called two-sided spreading and it occurs for negative values of $\hat{M}$ and small values of $\hat{N}$, which is the region marked I in figure 2. If both contact angles are less than the receding contact angle, then both contact lines will recede toward the centre of the droplet. This two-sided shrinking occurs in the region marked III in figure 2, which is for small $\hat{N}$ and $\hat{M}$ larger than some critical value. These two behaviours are in accord with the results of Ehrhard & Davis (1991) that say that uniform heating of the solid, $\hat{M} > 0$, reduces spreading while uniform cooling, $\hat{M} < 0$, promotes spreading. In between these two regions is a region marked II in which the contact angles are between

the advancing and receding contact angles. As a result, the contact lines are pinned and the bulk droplet stays motionless. However, there is still a thermocapillary flow inside the droplet, which produces an asymmetric shape.

In region IV of figure 2, $\hat{N}$ is large enough so that the left contact angle is between the advancing and receding angles, while the right contact angle is greater than the advancing contact angle. In this case, spreading occurs from the right side, but the left contact line is pinned on the solid. This is called one-sided spreading.

In region V, $\hat{M}$ is positive and large enough to reduce the left contact angle so that it is less than the receding angle and the right contact angle is reduced so that it is between the advancing and receding contact angles. Thus, one-sided shrinking occurs in which the right contact line is pinned and the left contact line recedes and reduces the width of the droplet.

For even larger values of the imposed temperature gradient, the left contact angle is reduced to a value less than the receding contact angle. Now, both contact lines will move to the right. This is the case of droplet migration. The speed of the contact lines is most likely different and so as the entire droplet moves, it also changes its width. In region VIa, the droplet begins to migrate, but it also stretches since the right contact line moves faster than the left. In region VIb, the droplet starts to shrink as it migrates. The asymptotic approximation of the boundary between stretching and shrinking is a straight vertical line as shown in figure 2. A second-order approximation is needed to bring in the curvature exhibited by the numerical result.

The last type of initial response is delineated by region VII of figure 2 and occurs when the droplet is strongly heated. If the model is taken seriously, the strong heating causes the left contact angle to be less than zero. A droplet shape computed in this region would have a free surface that intersects the solid at a point other than the contact line. This unphysical result shows that the present model fails to represent the true behaviour of the droplet. This type of breakdown of the lubrication model was also seen in the liquid film rupture studies of Burelbach, Bankoff & Davis (1990) and Tan, Bankoff & Davis (1990). The curve $\bar{\theta}_R = 0$ forms the lower boundary of this region. It is very difficult to compute numerically because the free-surface shape oscillates very rapidly in this region and so it is difficult to stay with any one particular root. This is evidenced by the slightly jagged nature of the curve. The asymptotic approximation of the curve $\bar{\theta}_R = 0$ is so inaccurate that it was not included in the figure.

There are several possibilities for the actual behaviour of the droplet in region VII: the droplet could still migrate at constant speed, a very thin film of liquid could form on the trailing edge of the droplet, the trailing film could rupture and form small droplets that appear to be shed from the main droplet, or the trailing film could just spread out the droplet into a very thin film on the solid. To investigate these possible behaviours, we must first modify our physical and/or numerical model. We could include additional physics into the model to prevent the free surface from penetrating the solid, such as van der Waals forces, or just completely abandon the lubrication model in this contact-line region. The numerical method may also be a fault and so we could use a technique that increases the local resolution of the computation in the left contact-line region. We shall not pursue these matters any further in this paper.

4.2. *Steady-state response*

Once a droplet begins to move according to the initial responses described above, its width will change. As the droplet stretches, the restriction of constant volume will force both contact angles to decrease. Shrinking causes both contact angles to increase. This

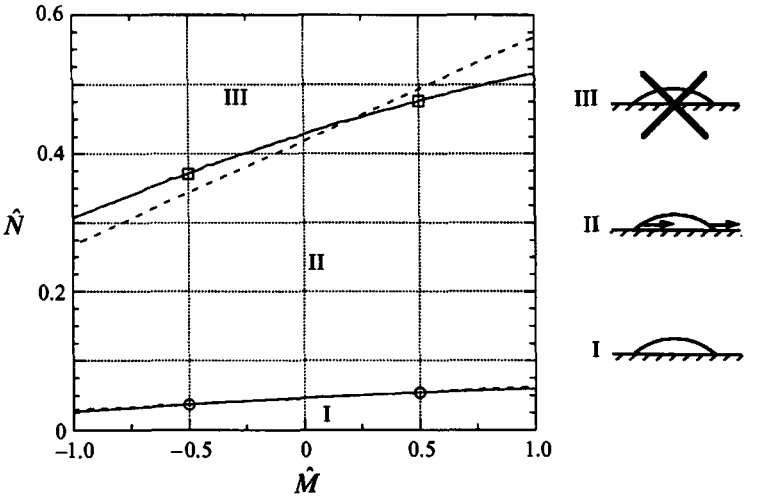

FIGURE 3. Parameter plot of $\hat{N}$ versus $\hat{M}$ for the steady-state behaviour of a droplet with $G = 0$, $\bar{\theta}_A = 1$, and $\bar{\theta}_R = 0.8$. Solid lines are the numerical results and dashed lines are the asymptotic approximations. Region I, no motion; II, constant-velocity migration; III, invalid model behaviour. ○, $\theta_r = \bar{\theta}_R$ and $\theta_a = \bar{\theta}_A$, which is the onset of droplet migration; □, $\theta_a - \bar{\theta}_A = \bar{\theta}_R - \theta_r$ and $\theta_r = 0$, which is the largest physically possible value of $\hat{N}$. The small droplet schematics to the right of the figure indicate the direction and relative magnitude of the contact-line motion in each of the marked regions.

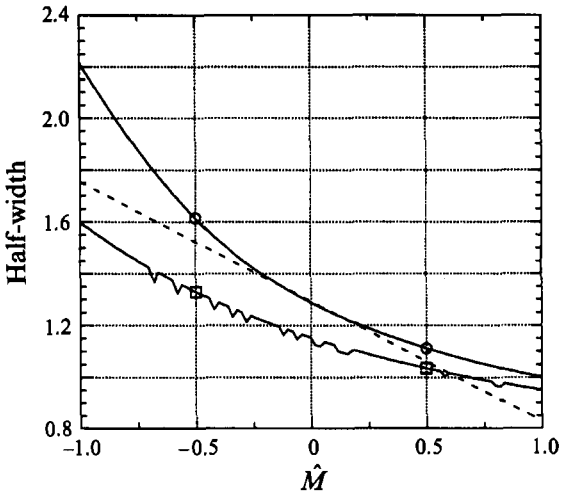

FIGURE 4. The half-width of a droplet corresponding to the two bounding curves shown in figure 3. Solid lines are the numerical results and the dashed line is the asymptotic approximation. ○, $\theta_r = \bar{\theta}_R$ and $\theta_a = \bar{\theta}_A$, which is the onset of droplet migration; □, $\theta_a - \bar{\theta}_A = \bar{\theta}_R - \theta_r$ and $\theta_r = 0$, which is the largest physically possible value of $\hat{N}$.

behaviour modifies the speed of each contact line, which in turn modifies the stretching or shrinking of the droplet. After a sufficiently long time, the droplet may reach a steady state. Figure 3 is a parameter plot of the steady-state response of a droplet. In region I, the droplet is motionless because both contact angles are between the advancing and receding contact angles. To reach this condition, the droplet may

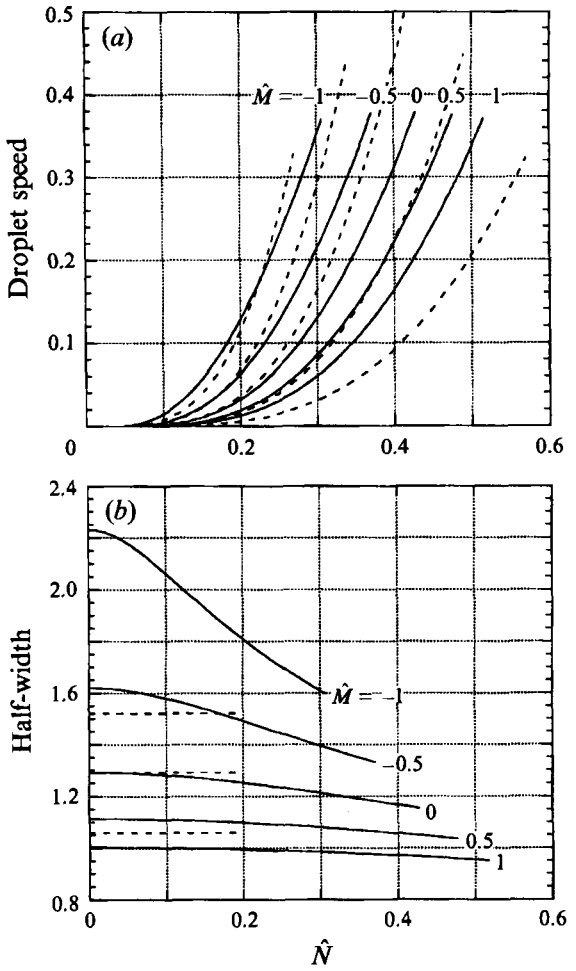

FIGURE 5. (*a*) The speed and (*b*) the half-width of a droplet, during constant-velocity migration, as a function of the imposed temperature gradient $\hat{N}$ for various values of the parameter $\hat{M}$ and with $G = 0$, $\bar{\theta}_A = 1$, and $\bar{\theta}_R = 0.8$. Solid lines are the numerical results and dashed lines are the asymptotic approximations.

spread or shrink or do nothing depending on the initial configuration. The boundary of this region is given by the two conditions $\theta_a = \bar{\theta}_A$ and $\theta_r = \bar{\theta}_R$. The asymptotic approximation of the boundary of this region is very good over the entire parameter range of $\hat{M}$ that was covered. In figure 4, the half-width of the droplet versus $\hat{M}$ corresponding to the curves shown in figure 3 are shown. As expected, the width of the droplet decreases as the solid surface is heated above the temperature of the passive gas, i.e. for increasing $\hat{M}$. The asymptotic approximation of the half-width is only accurate near $\hat{M} = 0$, in contrast to the previous figure.

In region II of figure 3, the droplet moves at a constant velocity. There is an initial transient during which the width of the droplet either increases or decreases until the speeds of both contact lines are identical. After this point the droplet moves without change of shape. The upper boundary of this region is given by the constant-velocity condition, $\theta_a - \bar{\theta}_A = \bar{\theta}_R - \theta_r$, plus the condition $\bar{\theta}_R = 0$. The corresponding half-width of the droplet at this boundary is given in figure 4. The asymptotic approximation of

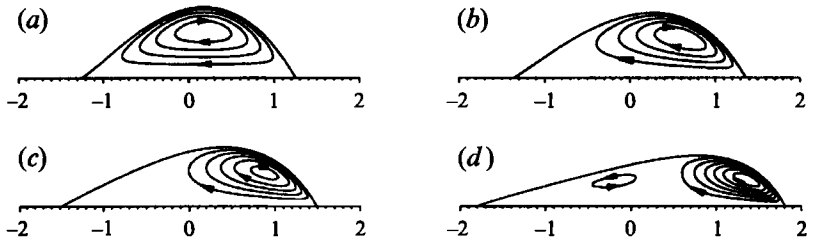

FIGURE 6. The streamlines ψ and the free-surface profile ($\psi = 0$) for a droplet in constant-velocity migration. The imposed temperature gradient is $\hat{N} = 0.2$, $\bar{\theta}_A = 1$, and $\bar{\theta}_R = 0.8$. The main recirculation cell has a clockwise rotation. The streamlines are plotted in increments of $\psi = -0.0006$, except where noted. (*a*) $\hat{M} = 0$, $\psi_{min} = -0.002825$, $\psi_{max} = 0$; (*b*) $\hat{M} = -0.25$, $\psi_{min} = -0.002914$, $\psi_{max} = 0$; (*c*) $\hat{M} = -0.5$, $\psi_{min} = -0.003232$, $\psi_{max} = 0.0001456$; and (*d*) $\hat{M} = -1.0$, $\psi_{min} = -0.004035$, $\psi_{max} = 0.0004605$. The small counterclockwise recirculation cell on the left of droplet (*d*) is plotted with the streamline $\psi = 0.0004$.

the curve $\hat{N}$ versus $\hat{M}$ in figure 3 is not very accurate, chiefly because $\hat{N}$ is not very small, and the half-width curve in figure 4 is so inaccurate that it was not included in the figure.

The region marked III in figure 3 is that in which the left contact angle is less than zero. As before, the model breaks down in this region and it is not investigated further in this paper.

The velocity of a migrating droplet versus $\hat{N}$ for various values of $\hat{M}$ is shown in figure 5(*a*). The corresponding half-width of the droplet is shown in figure 5(*b*). This figure shows that as the imposed temperature gradient increases, the speed of the droplet increases monotonically and its width decreases monotonically. Also, given a fixed value of the imposed temperature gradient $\hat{N}$, decreasing the overall heating of the droplet to the passive gas (decreasing $\hat{M}$) increases both the droplet migration speed and width.

The asymptotic approximation to the migration velocity is not very accurate for the larger values of $\hat{N}$ and $\hat{M}$ as shown in figure 5(*a*). Figure 5(*b*) shows that a second-order approximation is needed to more accurately capture the behaviour of the droplet width.

The flow field in a steady-state migrating droplet is shown in figure 6. In these plots, the imposed temperature gradient is held fixed at $\hat{N} = 0.2$, and $\hat{M}$ decreases meaning that there is an overall cooling of the droplet by the solid. In figure 6(*a*), $\hat{M} = 0$ and the flow in the droplet takes the form of one clockwise recirculating cell. The cell fills the entire droplet and the flow on the free surface is from the left to the right, or from the hot end to the cold end. As $\hat{M}$ decreases, the fluid velocity near the free surface on the right side of the droplet is increased and the velocity on the left is decreased as suggested by the results of Ehrhard & Davis (1991). The result is a distortion of the recirculation cell and the droplet shape as shown in figure 6(*b*, *c*). If the absolute value of $\hat{M}$ is large enough, an additional counterclockwise recirculation cell appears in the droplet as shown in figure 6(*d*). In fact, such a cell is present for the conditions of figure 6(*c*), but it is too small to see.

The difference between the advancing and receding contact angles, $\Psi = \bar{\theta}_A - \bar{\theta}_R$, is called the contact-angle hysteresis. It ranges from zero for $\bar{\theta}_A = \bar{\theta}_R = 1$, to one for $\bar{\theta}_A = 1$ and $\bar{\theta}_R = 0$. The effect of contact-angle hysteresis on the motion of a droplet for $\hat{M} = 0$ is shown in the steady-state parameter plot of figure 7, which is similar to that of figure 3. In region I, the distortion of the droplet due to the thermocapillary forces is insufficient to allow the contact lines to move after a transient period of spreading

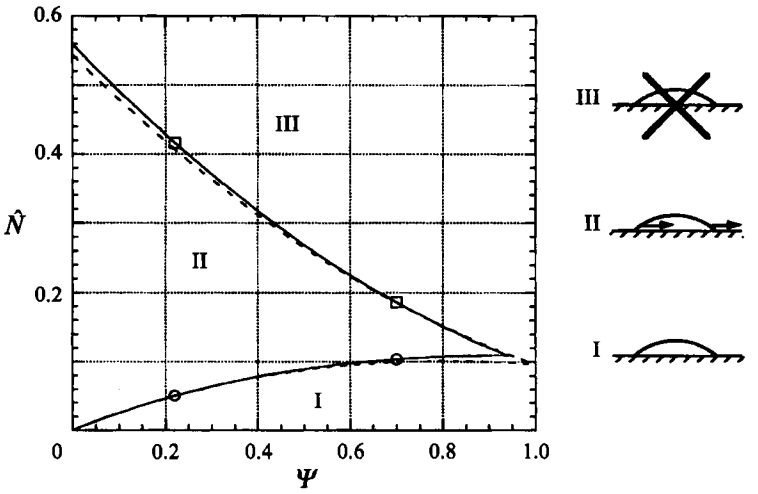

FIGURE 7. Parameter plot of $\hat{N}$ versus the contact-angle hysteresis Ψ for the steady-state behaviour of a droplet with $G = 0$, $\bar{\theta}_A = 1$, and $\hat{M} = 0$. Solid lines are the numerical results and dashed lines are the asymptotic approximations. Region I, no motion; II, constant-velocity migration; III, invalid model behaviour. ○, $\theta_r = \bar{\theta}_R$ and $\theta_a = \bar{\theta}_A$, which is the onset of droplet migration; □, $\theta_a - \bar{\theta}_A = \bar{\theta}_R - \theta_r$ and $\theta_r = 0$, which is the largest physically possible value of $\hat{N}$. The small droplet schematics to the right of the figure indicate the direction and relative magnitude of the contact-line motion in each of the marked regions.

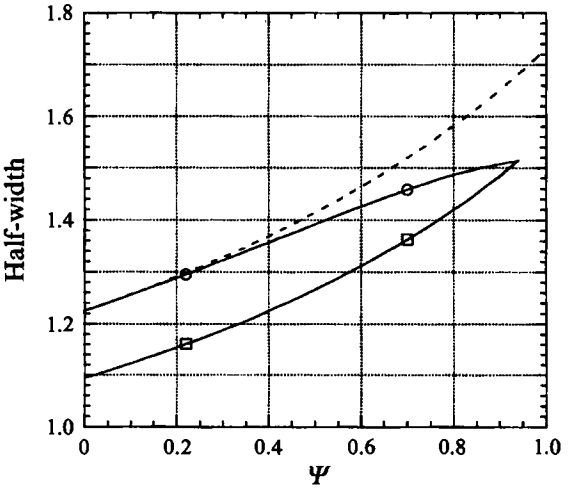

FIGURE 8. The half-width of a droplet corresponding to the two bounding curves shown in figure 7. Solid lines are the numerical results and the dashed line is the asymptotic approximation. ○, $\theta_r = \bar{\theta}_R$ and $\theta_a = \bar{\theta}_A$, which is the onset of droplet migration; □, $\theta_a - \bar{\theta}_A = \bar{\theta}_R - \theta_r$ and $\theta_r = 0$, which is the largest physically possible value of $\hat{N}$.

or shrinking. In effect, the contact-angle hysteresis is large enough to hold the droplet motionless. In region II, the applied temperature gradient produces a steady migration of the droplet. The model fails in region III because the left contact angle is less than zero. The half-width of the droplet corresponding to the two curves in figure 7 is shown in figure 8.

When the hysteresis is zero, the droplet is never motionless. The droplet migrates as soon as the temperature gradient is imposed, and it ultimately reaches a steady-state

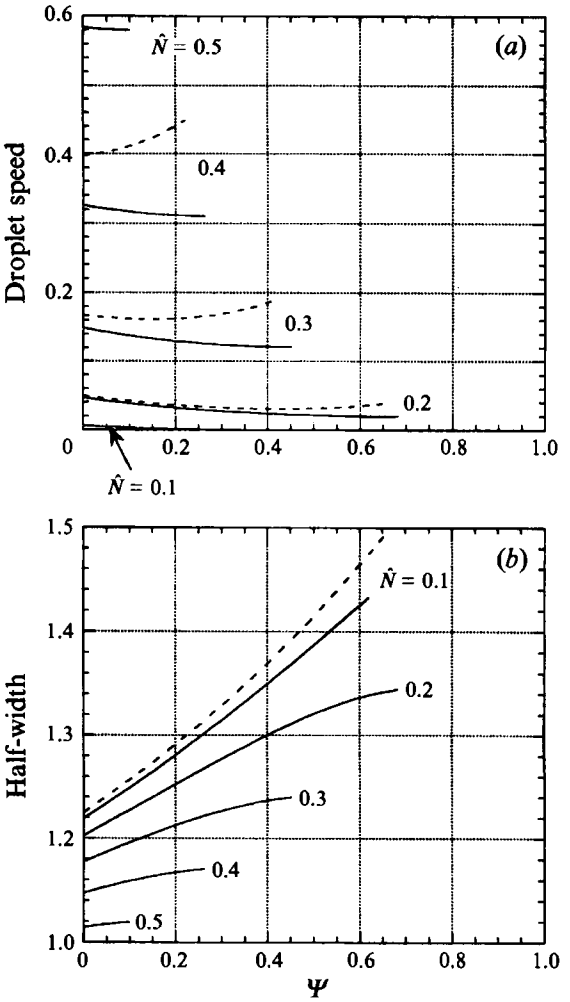

FIGURE 9. (*a*) The speed and (*b*) the half-width of a droplet, during constant-velocity migration, as a function of the contact-angle hysteresis Ψ for various values of the imposed temperature gradient $\hat{N}$ and with $G = 0$, $\hat{M} = 0$, and $\bar{\theta}_A = 1$. Solid lines are the numerical results and dashed lines are the asymptotic approximations.

speed for $\hat{N}$ not too large. As the hysteresis increases, the largest value of the applied temperature gradient and the corresponding droplet half-width for a motionless droplet increase. The upper limit for steady-state droplet migration decreases as the hysteresis increases. Thus, the range of possible values of $\hat{N}$ for a steady-state migration decreases. The numerical calculations show that for $0.94 < \Psi < 1$ there is no regime of steady-state droplet migration. However, this result will almost surely be modified once the model is augmented to remedy the computational difficulties seen in region III. The perturbation approximations shown in figure 7 are fairly accurate for the whole range of hysteresis. However, there is a slight maximum at $\Psi = 0.8$ in the lower curve that is not present in the numerical results, and the approximations show that there is no range of hysteresis where steady-state droplet migration is prohibited. The approximation for the droplet half-width in figure 8 is only good for the curve bounding the motionless droplet and for small values of the contact-angle hysteresis.

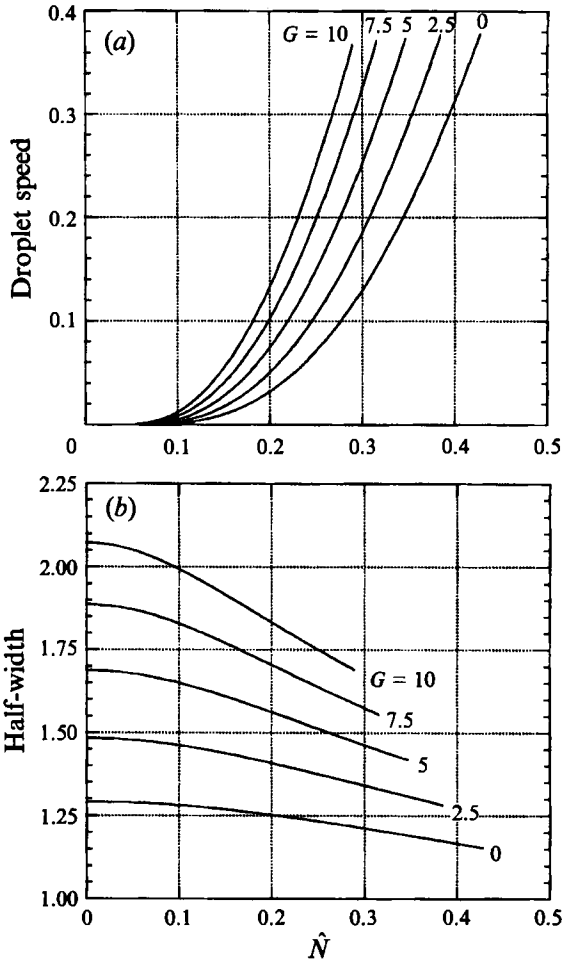

FIGURE 10. (*a*) The speed and (*b*) the half-width of a droplet, during constant-velocity migration, as a function of the imposed temperature gradient $\hat{N}$ for various values of the Bond number G and with $\hat{M} = 0$, $\bar{\theta}_A = 1$, and $\bar{\theta}_R = 0.8$.

Figures 9(*a*) and 9(*b*) show the droplet migration speed and half-width for a number of different values of $\hat{N}$ versus the contact-angle hysteresis. For a fixed value of the applied temperature gradient, the speed does not change much as the contact-angle hysteresis increases. Instead, the droplet half-width increases to accommodate the change. For a fixed value of the contact-angle hysteresis, the droplet speed increases and its half-width decreases as $\hat{N}$ increases as seen previously.

The effect of gravity on the migration speed and half-width of a droplet is shown in figures 10(*a*) and 10(*b*) for the case of $\hat{M} = 0$. For a fixed value of $\hat{N}$, increasing gravity increases both the width and the migration speed of the droplet.

4.3. *Transient response*

The transient response of the droplet is given by the solution of the contact-line differential equations (13*c*, *d*). The sum and difference of these equations yield first-order differential equations for the half-width $a(t) = \frac{1}{2}(c_a - c_r)$ and the centreline position $\bar{c}(t) = \frac{1}{2}(c_a + c_r)$ of the droplet. These two differential equations are solved numerically using either the perturbation approximation or the numerical solution for

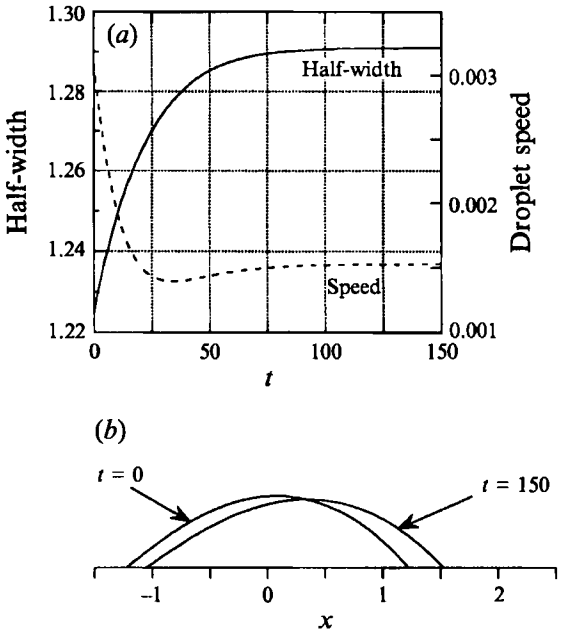

FIGURE 11. The transient response of a droplet based on the perturbation approximation. The imposed temperature gradient $\hat{N} = 0.1$ and $\hat{M} = 0$, $\bar{\theta}_A = 1$, and $\bar{\theta}_R = 0.8$. (*a*) The droplet half-width and the droplet speed versus time t, and (*b*) the free-surface profiles at $t = 0$ and 150.

the contact angles. The results of such a calculation using the perturbation approximation with $\hat{M} = 0$ and $\hat{N} = 0.1$ and with an initial width of a fully spread isothermal droplet are shown in figure 11. These parameter values correspond to an initial state of one-sided spreading and a final state of steady migration. In figure 11 (*a*), the droplet half-width is seen to increase monotonically to its final value. Intermediate results not shown in the figure indicate that one-sided spreading occurs during the time interval (0, 2.75). After this, the droplet migrates to the right and stretches. Also shown in figure 11 (*a*) is the droplet speed, which decreases from its initial value and then slightly undershoots its final value.

Two droplet profiles are shown in figure 11 (*b*). The first is the initial shape. This is slightly asymmetric because of the imposed temperature gradient. The second profile is for the dimensionless time of $t = 150$, which is well into the domain of steady-state migration of the droplet. Here, the droplet is slightly wider and more asymmetric, and the centreline has only migrated 0.235 dimensionless units to the right. This small migration is due to the very small migration speeds, and at least for this case, it supports the neglect of the term $\hat{N}x$ in the evolution equation.

Figure 12 shows a transient calculation with $\hat{N} = 0.2$. For this value of $\hat{N}$, the initial and final behaviour is droplet migration. Both the droplet half-width and speed increase monotonically to their final values. However, the droplet speed stays almost constant during the first few units of time. In figure 12 (*b*), the initial droplet profile is shown. It is slightly more asymmetric than the previous case because of the larger value of $\hat{N}$. The droplet speed is much larger in this case and so the droplet centreline has migrated a distance of 0.863 dimensionless units over 25 units of time as shown.

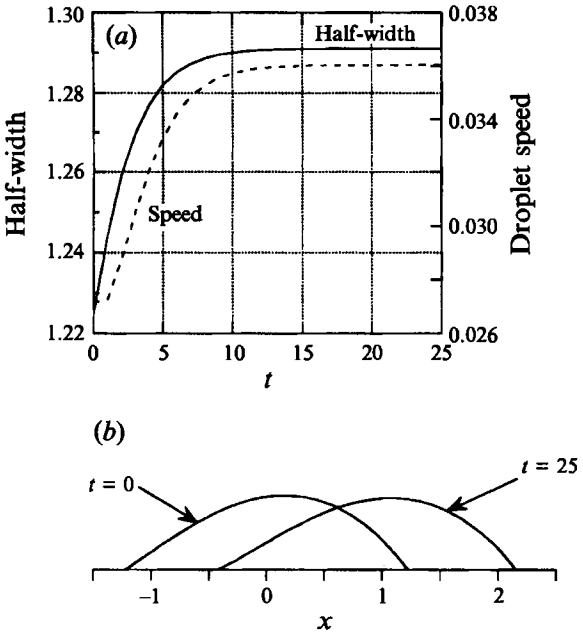

FIGURE 12. As figure 11, but for $\hat{N} = 0.2$. (*a*) The droplet half-width and the droplet speed versus time t, and (*b*) the free-surface profiles at $t = 0$ and $t = 25$.

5. Conclusions

The behaviour of a two-dimensional liquid droplet on a horizontal solid surface with an imposed temperature gradient has been explored. The droplet is composed of a viscous liquid and is thin enough so that lubrication theory can be applied. The result is an evolution equation for the shape of the free surface of the droplet. This is coupled to a dynamic contact-line boundary condition relating the contact-line speed and the apparent contact angles that governs the motion of the contact lines. The mobility capillary number is assumed small and so the short transient associated with the evolution of the free surface for a fixed droplet width is ignored. Subsequent evolution of the free surface is determined by the motion of the contact lines. This theory gives a good approximation to the flow in the droplet, the shape of the free surface, and the motion of the contact lines.

When a temperature gradient is applied to a droplet of a given width placed on a solid surface, a number of different initial contact-line behaviours may occur that depend on the two thermal parameters $\hat{M}$ and $\hat{N}$ characterizing the heating. These behaviours include motionless contact lines, one- or two-sided spreading or shrinking, or migration of the entire droplet. After a transient period of a length that depends on the magnitude of the imposed heating, the droplet may remain motionless, or migrate down the temperature gradient with a constant shape. For large enough heating, a serious interpretation of the model says that one or both of the contact angles may become less than zero. In this case, the present model does not apply because there is no built-in mechanism to prevent this unphysical event from occurring. The behaviour under these conditions of intense heating is open to speculation and further exploration.

The contact-line motions described above are produced by the fluid flow inside the droplet. The temperature gradient imposed on the solid surface produces a thermocapillary flow in the droplet that is directed along the free surface from the hot

contact line to the cold contact line. As this flow approaches the cold contact line, it is deflected back along the solid surface toward the hot end of the droplet. The resulting recirculation cell has a zero net mass flux at any vertical cross-section of the droplet. The deflection of the flow at the cold end of the droplet sets up a pressure gradient inside the droplet that drives the return flow and distorts the free surface. This distortion increases the contact angle at the cold end of the droplet and decreases the contact angle at the hot end. These changes in the contact angles force the motion of the contact lines through the dynamic contact-line boundary condition posed for this model. If the imposed temperature gradient is large enough, both contact lines will move in the direction of decreasing temperature.

The single thermocapillary recirculation cell set up by the imposed temperature gradient becomes distorted because of thermal variations established by the heat transfer from the droplet to the surrounding passive gas. This is the effect studied by Ehrhard & Davis (1991). With no imposed temperature gradient in the solid, the heat transfer to a droplet that is colder than the surrounding gas produces a symmetric temperature variation along the free surface from the hotter top of the droplet to the colder contact lines. This thermal variation produces two thermocapillary recirculation cells, with the one on the right rotating in the clockwise direction and the one on the left rotating in the counterclockwise direction. When combined with the single recirculation cell produced by an imposed temperature gradient in which the temperature decreases to the right, the resulting thermocapillary flow is intensified on the right and decreased on the left. This shifts the centre of the recirculation cell toward the right side of the droplet as shown in figure 6. This modified flow field alters the contact angles in the droplet, and thereby changes the motion of the contact lines.

The most interesting and perhaps useful behaviour seen in this work is the steady-state migration of the droplet down the imposed temperature gradient. Increasing this temperature gradient (larger $\hat{N}$) increases the droplet speed and decreases its width. A decrease in the overall heating of the droplet by the solid (decreasing $\hat{M}$) increases both the droplet speed and its width. This observation is consistent with the results of Ehrhard & Davis (1991) and Ehrhard (1993), which say that droplet cooling ($\hat{M} < 0$) promotes spreading, leading to larger droplets, and heating ($\hat{M} > 0$) inhibits spreading, leading to smaller droplets. Increasing the contact-angle hysteresis of the droplet increases the value of $\hat{N}$ needed to produce a steady migration, but decreases the value of $\hat{N}$ at which the model fails. Once the droplet is migrating at a constant velocity, increasing the contact-angle hysteresis does not change the speed much, but the droplet width increases. Finally, an increase in the gravitational body force measured by the Bond number G increases both the droplet migration speed and its width, as might be expected since gravity would tend to flatten the droplet.

One of the more arbitrary assumptions made in this paper was to neglect the $\hat{N}x$-term in the evolution equation (10). A qualitative understanding of the effect of this term on the motion of a steady migrating droplet starts with noting that as the droplet moves down the solid in the direction of decreasing temperature, it experiences a larger overall cooling by the solid that is equivalent to a decrease in $\hat{M}$. From figure 5(*a*), decreasing $\hat{M}$ for a fixed $\hat{N}$ causes the droplet speed and width to increase. Thus, the effect of the $\hat{N}x$-term is to accelerate and widen the droplet as it moves down the imposed temperature gradient on the solid surface.

A physical way to eliminate the effect of the $\hat{N}x$-term is to impose the same temperature gradient on both the solid and the gas above the droplet so that there is always a constant temperature difference between the two. In this situation, the $\hat{N}x$-term does not appear in the final evolution equation.

Appendix. Perturbation approximations

Consider the initial shape of a droplet with a given half-width a. The perturbation approximation to the line $\theta_a = \theta$, where θ is either $\bar{\theta}_A$, $\bar{\theta}_R$, or 0 is

$$\hat{N} = \hat{M}\left[\frac{1}{2a^2} - \frac{1}{3}\left(\theta - \frac{3}{2a^2}\right)\right] + \frac{1}{a^3}\left[\theta - \frac{3}{2a^2}\right]. \tag{A 1}$$

The perturbation approximation to the line $\theta_r = \theta$ is

$$\hat{N} = \hat{M}\left[-\frac{1}{2a^2} + \frac{1}{3}\left(\theta - \frac{3}{2a^2}\right)\right] - \frac{1}{a^3}\left[\theta - \frac{3}{2a^2}\right]. \tag{A 2}$$

For a droplet with the contact angles $\bar{\theta}_A = 1$ and $\bar{\theta}_R = 0.8$ and with a half-width of $a = (3/2\bar{\theta}_A)^{1/2} = (3/2)^{1/2}$, the lines shown on figure 2 are

$$\theta_a = \bar{\theta}_A \Rightarrow \hat{N} = \hat{M}/3, \tag{A 3}$$

$$\theta_a = \bar{\theta}_R \Rightarrow \hat{N} = (0.4)\,\hat{M} - 0.108866, \tag{A 4}$$

$$\theta_a = 0 \Rightarrow \hat{N} = 2\hat{M}/3 - 0.544331, \tag{A 5}$$

$$\theta_r = \bar{\theta}_A \Rightarrow \hat{N} = -\hat{M}/3, \tag{A 6}$$

$$\theta_r = \bar{\theta}_R \Rightarrow \hat{N} = -(0.4)\,\hat{M} + 0.108866, \tag{A 7}$$

$$\theta_r = 0 \Rightarrow \hat{N} = -2\hat{M}/3 + 0.544331. \tag{A 8}$$

In region VI of figure 2, the droplet immediately begins to migrate. It will tend to stretch if the speed of the right contact line is larger than the speed of the left contact line. This is given by the relation $\theta_a - \bar{\theta}_A \geqslant \bar{\theta}_R - \theta_r$. The perturbation approximation for stretching is thus

$$\hat{M} \leqslant \frac{1}{a}[3/a^2 - \bar{\theta}_A - \bar{\theta}_R]. \tag{A 9}$$

For the present special case, this is $\hat{M} \leqslant 0.163299$. Note that for this curve, a higher-order approximation is needed to capture the behaviour of the system.

Figure 3 is a domain map showing the steady-state response of the system. The boundary of region I for a motionless droplet is given by $\theta_a = \bar{\theta}_A$ and $\theta_r = \bar{\theta}_R$. This gives a perturbation approximation for the droplet half-width and the applied temperature gradient of

$$a = a_0 - a_0^4\,\hat{M}/6, \quad a_0 = [3/(\bar{\theta}_A + \bar{\theta}_R)]^{1/2}, \tag{A 10}$$

$$\hat{N} = \tfrac{1}{2}(\bar{\theta}_A - \bar{\theta}_R)\,[1/a_0^3 + \hat{M}/6]. \tag{A 11}$$

For the present special case, this yields

$$a = 1.290994 - 0.462963\,\hat{M}, \tag{A 12}$$

$$\hat{N} = 0.0464758 + 0.0166667\,\hat{M}. \tag{A 13}$$

Region II of figure 3 is constant-speed droplet migration. This is given by the equation $\theta_a - \bar{\theta}_A = \bar{\theta}_R - \theta_r$. The droplet half-width in this case is also given by equation (A 10). The droplet speed V is

$$V = \{-\tfrac{1}{2}(\bar{\theta}_A - \bar{\theta}_R) + a_0^3\,\hat{N}[1 - a_0^3\,\hat{M}/6]\}^m. \tag{A 14}$$

Finally, region III of figure 3 is unknown because the rear contact angle is less than zero. The boundary of the region is given by the line $\theta_r = 0$ and the constant-speed

equation $\theta_a - \bar{\theta}_A = \bar{\theta}_R - \theta_r$. This results in a droplet half-width still given by equation (A 10), and an imposed temperature gradient of

$$\hat{N} = \tfrac{1}{2}(\bar{\theta}_A + \bar{\theta}_R)[1/a_0^3 + \hat{M}/6]. \tag{A 15}$$

For the present special case, this yields

$$\hat{N} = 0.418282 + 0.15\hat{M}. \tag{A 16}$$

REFERENCES

BOYD, J. P. 1989 *Chebyshev & Fourier Spectral Methods*. Lecture Notes in Engineering, Vol. 49. Springer.

BURELBACH, J. P., BANKOFF, S. G. & DAVIS, S. H. 1990 Steady themocapillary flows of thin liquid layers. II. Experiment. *Phys. Fluids* A **2**, 322–333.

CHAUDHURY, M. K. & WHITESIDES, G. M. 1992 How to make water run uphill. *Science* **256**, 1539–1541.

CHEN, J. 1988 Experiments on a spreading drop and its contact angle on a solid. *J. Colloid Interface Sci.* **122**, 60–72.

DUSSAN V., E. B. 1979 On the spreading of liquids on solid surfaces: static and dynamic contact lines. *Ann. Rev. Fluid Mech.* **11**, 371–400.

DUSSAN V., E. B., RAMÉ, E. & GAROFF, S. 1991 On identifying the appropriate boundary condition at a moving contact line: an experimental investigation. *J. Fluid Mech.* **230**, 97–116.

EHRHARD, P. 1993 Experiments on isothermal and non-isothermal spreading. *J. Fluid Mech.* **257**, 463–483.

EHRHARD, P. & DAVIS, S. H. 1991 Non-isothermal spreading of liquid drops on horizontal plates. *J. Fluid Mech.* **229**, 365–388.

GENNES, P. G. DE 1985 Wetting: statics and dynamics. *Rev. Mod. Phys.* **57**, 827–863.

GREENSPAN, H. P. 1978 On the motion of a small viscous droplet that wets a surface. *J. Fluid Mech.* **84**, 125–143.

HALEY, P. J. & MIKSIS, M. J. 1991 The effect of the contact line on droplet spreading. *J. Fluid Mech.* **223**, 57–81.

HOCKING, L. M. 1983 The spreading of a thin drop by gravity and capillarity. *Q. J. Mech. Appl. Maths* **36**, 55–69.

HOCKING, L. M. 1992 Rival contact-angle models and the spreading of drops. *J. Fluid Mech.* **239**, 671–681.

HOCKING, L. M. & RIVERS, A. D. 1982 The spreading of a drop by capillary action. *J. Fluid Mech.* **121**, 425–442.

MARSH, J. A., GAROFF, S. & DUSSAN V., E. B. 1993 Dynamic contact angles and hydrodynamics near a moving contact line. *Phys. Rev. Lett.* **70**, 2778–2781.

NGAN, C. G. & DUSSAN V., E. B. 1989 On the dynamics of liquid spreading on solid surfaces. *J. Fluid Mech.* **209**, 191–226.

ROSENBLAT, S. & DAVIS, S. H. 1985 How do liquid drops spread on solids? In *Frontiers in Fluid Mechanics* (ed. S. H. Davis & J. L. Lumley), pp. 171–183. Springer.

TAN, M. J., BANKOFF, S. G. & DAVIS, S. H. 1990 Steady thermocapillary flows of thin liquid layers. I. Theory. *Phys. Fluids* A **2**, 313–321.

TANNER, L. H. 1979 The spreading of silicone oil drops on horizontal surfaces. *J. Phys.* D: *Appl. Phys.* **12**, 1473–1484.